SEISMIC INVESTIGATION OF BAUXITE LENSES AHEAD OF THE GALLERIES AT A BAUXITE MINE- CENTRAL GREECE

G-AkisTselentis[(1)], Paraskevas Paraskevopoulos[(1)] and Nikolaos Martakis[(2)]

(1) University of Patras, Seismological Laboratory, Rio 26504, Greece

(2) LandTech Enterprises, Athens Greece

ABSTRACT

This paper describes the methodology and the results of a seismic geophysical investigation of Bauxite lenses ahead of galleries in the prospects of a Bauxite mine in central Greece. The methods used were equi travel plane seismic reflection imaging and seismic tomography.

Measurements were performed on a known deposit, verified by exploratory drilling and the obtained results indicate that these methodologies have a strong potential in Bauxite exploration and mining and can reduce significantly the drilling costs.

INTRODUCTION

Geological prediction ahead of mining galleries and tunnels is of outmost importance in minning and tunnelling and is a leading international topic and problem all over the world. While horizontal exploratory boring conducted from a gallery face provides good accuracy, they are costly and time-consuming.

The application of underground geophysical investigations can provide important information for resource estimation, security and cost of tunnel or gallery construction. An

important feature of the geophysical imaging ahead of a gallery face must be the rapid turn-around from data acquisition to analysis and precision of results. Ideally geophysical data acquisition should not interrupt the mining operations and data should be processed on-site and the geological interpretations should be available within 1 or 2 days.

Many geophysical techniques have been developed and applied to predict the geological conditions ahead of the advancing gallery face, during the past few years. These techniques include electrical methods (e.g Tsai 2005a), seismic methods (e.g Ashida 2001, Otto et al., 2002) and electromagnetic methods (e.g. Grodner 2001). In electrical methods, and in particular electrical tomography, the electrical resistivity is used to briefly determine geological discontinuities and ore bodies for a few tens of meters investigation range. In electromagnetic methods mainly encountering Ground Penetration Radar (GPR) measurements, electromagnetic pulses are emitted and captured to detect geological discontinuities (e.g. Grodner 2001).

Tunnel seismic prediction techniques are based on detecting reflective signals due to geological heterogeneities caused by the impedance mismatch (Sattel, 1992). According to these techniques, seismic receivers and sources are installed at the face and the side walls of the mining galleries. Various methodologies have been proposed such as horizontal seismic profiling (Imazaki et al., 1999), the tunnel seismic prediction (TSP) method (Tsai et al., 2005b; Lin et al., 2006), vertical seismic profiling (Bruckl et al., 2001), three-component seismic reflection surveys (Ashida 2001; Ashida et al., 2001; Yamamoto et al., 2010), Fresnel volume migration (Lüth et al., 2005), true reflection tomography (Otto et al., 2002) and seismic cross-hole velocity and attenuation tomography.

Dragicevic et al., 1991, applied the shallow seismic reflection method for locating Bauxite deposits at the Dinarides-Yougoslavia region. Neishtadt et al., 2006 developed a

seismoelectric method based on the Seismoelectrokinetic effect to search for Bauxite deposits. This method proved in some cases to differentiate Bauxites and kimberlites from host rock by their electrokinetic properties. Tsourlos et al., 2005 attempted to delineate Bauxite lenses using electrical tomography trechniques and GPR. Bi, 2009 applied the intermediate gradient method, Induced Polarization (IP) sounding method and resistivity method for the location of Bauxite deposits in western Hellan region, China. As far as seismic ahead of the mining galleries and seismic tomography methods, are concerned, the present work is the first time that these are applied in Bauxite exploration.

GEOLOGY

The mine where the present experiment was performed is located in central Greece in the area of the mountain of Ghiona (Figure 1a). The bauxite mine is in the exploitation phase and is located in the Variani area. The mine galleries are excavated from the mountain flanks with the main ones, leading to the ore, dipping downwards. After reaching the level of the ore the exploitation method used was mechanised “Room and pillars”. This means that there is already a number of tunnels excavated in and surrounding the ore region.

Geologicaly, the ore is in the isopic zone of Parnassos –Ghiona. The geologic formations that were encountered in the investigation site are presented in Figure 1b. The lithological column shows that the Bauxite lenses are to be found within the limestone layers. In general, the top of the ore is flat and is only tectonically disturbed in places. The floor in contrast is irregular with important elevation variation caused by the Karstic features containing the Bauxite ore. Similarly the walls of the ore usually follow the doline form having a circular or oval shape even though in more rare cases it has an irregular shaped perimeter. The walls are steeply dipping and they are often vertical, while the floor is irregular. In many cases the transition from limestone to Bauxite is not sharp but gradual with the presence of usually thin beds of

"grey Bauxite" (Tsourlos et al., 2005). In general the strike of the layers is from East to West dipping at about 20° N. Regarding the tectonic features of the area, there are thrust systems almost parallel to the strike of the geological strata, and faults that are vertical to it. The fault planes are usually not alterated except in some cases where zones of silt and clays are present. The presence of water in these discontinuities is limited in most cases.

METHODOLOGY

The first method which we used was the ahead of tunnel 3 Component geophone seismic imaging in order to locate the main seismic reflecting boundaries/planes. Because of the existing geometry of the galleries, we were also able to conduct a 2D tomographic survey that can delineate the areas where the seismic velocity changes showing areas where the lithology or the properties of the geological layers (eg. presence of faults) change.

Tunnel face seismic survey

The basic concept of the adapted methodology used is based on the work of Ashida (2001) and is presented in Figure 2. A seismic wave is generated by a seismic source placed in the face of the tunnel. Eight geophones (four 3-component geophones placed at each side wall of the tunnel), detect the seismic signal reflected from a geological boundary or discontinuity ahead of the tunnel face. Assuming an average seismic velocity of the ground, it is possible to draw an ellipsoid, which represents an equi-travel time surface. Every seismic ray that starts from the source and ends at the receiver after being reflected in any point of the ellipsoid will have an equal propagation time.

Let us consider the coordinate system shown in Figure 3, where the seismic source and receiver coordinates are transformed in such a way that they form an axis with the origin

located at the midpoint between them. If L is the source to reflector and back to receiver distance, V the velocity of the reflected wave and T_r the recorded travel time, we can write

$$L=V\ T_r \qquad (1)$$

Let $P(X_P,Y_P,Z_P)$; $S(X_S,Y_S,Z_S)$ and $R(X_R,Y_R,Z_R)$ the coordinates of the reflector, source and receiver respectively. Then, eq.1 can be written as

$$L = [(X_P - X_s)^2 + (Y_P - Y_s)^2 + (Z_P - Z_s)^2]^{1/2} + [(X_P - X_R)^2 + (Y_P - Y_R)^2 + (Z_P - Z_R)^2]^{1/2} \qquad (2)$$

From which we can write

$$\frac{X_P^2}{L^2 - 4Z_S^2} + \frac{Y_P^2}{L^2 - 4Z_S^2} + \frac{Z_P^2}{L^2} = \frac{1}{4} \qquad (3)$$

This equation represents an ellipsoid with the receiver R and the source S as foci. Thus, we can consider that the reflector P is a trace of points having the sum of distances to the receiver and source constant, or if we consider an average constant seismic velocity, the reflector point P lies on an equi-travel time plane. In the case of many source-receiver pairs we can construct the corresponding ellipsoids with the reflection plane being defined by the common to the ellipsoids tangent plane.

In the present implementation the above principle is used to map the processed seismic records avoiding the need for manually picking reflection arrival times. With this procedure the traces with the same phase will be stacked and amplified (towards their common tangent reflector plane) while they are attenuated elsewhere (Ashida, 2001).

If only one component were used the information would be limited to the amplitude component of the wave in one direction limiting the ability to know the true propagation direction. Utilizing the 3C records it is possible to estimate the direction of incidence and using it enhance seismic energy arriving from or close to, this direction, of the reflection point (Ashida, 2001). This can help in reducing the interference of seismic noise originating from other directions and limit imaging of false reflectors that could result from that.

APPLICATION

The measurements for a real data experiment were made at one of the mining galleries of a Bauxite mining company in central Greece. Figure 4 presents the survey setup. Four, 3-component geophones of the same type with a natural frequency of 28Hz were placed at each one of the side walls of the gallery (8 geophones in total) at an approximate height of 1m from the floor with the closest geophone (G4) at ~8 meters from the source position in the front. The z,y,x directions of each 3-component geophone are oriented to gallery axis direction, vertical to the gallery wall direction and vertical to the gallery floor direction respectively. The recording parameters and the used equipment are presented in Table 1.

As seismic source we used zero time detonating caps which were placed within boreholes having the depths of approximately 2m but different dips at the face of the gallery. The equipment setup and surveying are done prior to the measurements without interrupting the excavation cycle. Before the survey, during a drilling cycle, the geophones are installed at the walls of the gallery, the cables are laid out, and the source and geophone positions are accurately surveyed.

The excavation works were stopped during the measurements which consist of up to 3-5 recordings for each source location allowing the data to be stacked to increase the signal to noise ratio (SNR). The data acquisition lasts for approximately 20 min after which the mining

activities can resume while the survey equipment is removed. Data processing and reflector mapping can be performed near the worksite, using a portable computer, within several working hours.

Finally after the seismic sources were activated (shots), two source positions were used (D1 and D2 in Figure 4) that were relatively close to each other (~0.5m distance on the horizontal plane) on the plane but were at different elevations (D1 was 1.5 m above D2). A typical field record for one single shot is depicted in Fig.5. A “ringing” at frequencies slightly below 500Hz can be seen and this can be attributed to the vibration of the geophones. This “ringing” is higher than the frequencies of the reflected energy as measured in the traces of the other two components.

Table 2 presents the data processing flow which was used in the present experiment. AGC is performed to compensate the amplitude decay of the seismic signals due to transmission loss, spherical divergence and absorption. The previously mentioned “ringing”, which could mask the reflected waves, was suppressed by including into the processing flow a predictive deconvolution stage. Fig.6 presents the seismic section of Fig.5 after applying the processing flow described in Table 2. It can be seen that the “ringing” has been suppressed.

Before applying the imaging algorithm an average velocity for the medium has to be estimated. The value was estimated using the tomography result and in cases that tomography results are not available the first arrivals from the source to the geophones were used for estimating the average velocity. Based on the above a value of 3500 m/sec was used.

Each source point is imaged separately and the final results can be stacked together. Fig.7 a and b show 3D view of the results from different angles with two vertical intersecting planes each. Figure 7c shows the equi travel times imaging on a horizontal plane at X The lines indicate the interpreted positions of reflections. Figure 7d presents the vertical plane

marked in 7a and 7e presents a 2D view of the vertical plane marked in 7b at -22m on the y-axis. Figure 8 shows the 3D result of the equi-travel time plane imaging.

These figures show several areas of interest in the imaging result. On the left side (positive Y values) of the tunnel from Y axis 0 up to 22 m there is presence of a strong closely spaced equi-travel time planes indicating a rapid change in the medium probably a fault zone or small alternating layers. Further ahead, (increasing Z values) several distinct equi-travel time planes are present with a strong one at ~35 meters from the source while the most distant one is encountered at approximately 80 meters, indicating the presence of more abrupt reflectors.

Outside of the area of interest, in the positive part of the axis Y (right side of the tunnel) there is a presence of several strong reflectors indicating possible lithological changes or the presence of a fault.

Seismic tomography

Tomographic imaging is a noninvasive technique that has been successfully applied in a wide range of applications that span from medical imaging, to imaging the interior structure of the Earth (Nolet, 1987).

In brief, the theory of the tomographic technique used is as follows: Initially the area under investigation is divided by a grid. The dimensions for the cells of the grid are detemined in such a way that there is sufficient seismic ray coverage for each cell (in this case the coverage allowed us to have a 2x2 m grid). In order to obtain reliable results, a good ray coverage of the medium to be investigated is required. To achieve this, we need a good

positioning of sources and receiver. In addition to adequate ray coverage of the medium, it is important that the rays intersect the cells from different angles.

The travel time of the seismic ray between the source and the recording receiver can be analysed as the sum of the travel times through every cell of the grid. If the seismic source is at point S and the geophone at R, the travel time of the signal can be written as:

$$t_{S,R} = \int_{L_{S,R}} \frac{1}{V(x,y)} ds \qquad (4)$$

Which after discretization can be written as:

$$T_{S,R} = \sum_i \sum_j \frac{1}{V_{i,j}} \Delta S_{i,j,S,R}. \qquad (5)$$

In order to take into account the effect of the medium's velocity a ray tracing algorithm should be utilized. In our case we used the shortest ray path algorithm as proposed by Moser (1991) and modified by Zhang and Toksoz, (1998).

The next stage is to invert the obtained measurements using the non linear least squares inversion methodology of Zhang and Toksoz, (1998). In brief, to this methodology we iteratively change the velocity model parameters in order to minimize the difference between model values and data for the average slowness (travel time/raypath length) as well as the apparent slowness (slope of the travel time curve). This methodology also minimizes model "roughness" by utilizing Tikhonov's regularization as outlined in Zhang and Toksoz, (1998).

APPLICATION OF TOMOGRAPHY

The seismic tomography survey setup is presented in figure 9 depicting the location of seismic sources and receivers. The existing gallery geometry permitted the placement of 60 geophone - receiver positions at a spacing of 2 m. The geophones used had a natural

frequency of 60Hz and were placed at the gallery walls. As a seismic source we used a 5 Kg hammer and a metallic plate, stacking 7-10 blows in order to increase the S/N. In total, 11 seismic source locations were used, at a spacing of 12 m. The sampling interval and the seismic record length were kept the same as for the ahead of tunnel 3C survey.

First arrivals of P waves were measured on the raw seismic records. Figure 10 shows 2 select raw seismic records at locations 6 and 36 (as seen on figure 9) indicative of the raw data recorded.

A grid cell resolution of 2 x 2 meters for the inversion, was decided based on checkerboard tests and by comparing the ray coverage maps resulting from different resolutions. The inversion was performed using as starting model either a homogenous velocity model (the same that was used for the 3C imaging) or a simple velocity laterally changing model based on a preliminary investigation of the first arrivals of source receiver pairs with little differences in the final result. The obtained 2D tomography result gives a detailed view of the velocity distribution and is presented in Figure 11.

Judging from this figure we can see the presence of a rapid velocity decrease in the main tunnel between geophone positions 9-14. Optical observation on the wall tunnel by the mines geologists (personal communication) confirmed the presence of a lithological change within the limestone in these positions not related to bauxite. The slowest velocities 1000 -1800 m/sec corresponded with a fault zone in geophone positions 39-45 and filled in excavated part 59-60. Finally intermediate velocities 2000-2500 m/sec in geophone positions 53-54 where Bauxite was detected.

COMBINED RESULTS

In order to have a more complete interpretation, the results from both methods were combined in the excavation plane and were integrated and compared with the in situ observations and drilling results.

Figure 12a shows the result of the seismic imaging ahead of tunnel, for the excavation plane, overplotted on the 2D seismic tomography result. Figure 12b also shows the tangent reflector planes corresponding to the equi travel time planes.

The low velocity area with the rapid succession of reflectors as indicated by the arrow A was confirmed to be a fault alterated zone. The reflection dipping downwards shown by arrow B, that coincides with the end of the intermediate velocities, indicated the end of the Bauxite zone. It was later confirmed, by continuing the excavating tunnel that the Bauxite was indeed dipping downwards in the indicated position. The equi travel time planes in C and D were verified by the results of exploration drilling which showed the presence of fault planes in these positions.

CONCLUSIONS

In the present paper we examined the potential of two seismic methodologies on assessing Bauxite deposits ahead or between galleries. Reflection seismic ahead of gallery face seismic imaging can be a very useful tool in predicting geological conditions ahead during an active mine exploitation. The raw data and the results show that a high frequency dataset can be obtained inside the mine. We must note that the fact that the reflector plane is tangent to the equi travel times imaging, can cause some ambiguity in the interpretation of the results

Furthermore if combined with the use of seismic tomography can increase the accuracy of the results and significantly reduce the exploration drilling cost by optimizing the location of the excavating galleries in order to pass through the zones of interest.

ACKNOWLEDGEMENTS

We are grateful to Prof. Y. Ashida for providing us with the reflector geometrical imaging code and for his helpful advice during the course of the present investigations. We also thank S&B mines for permitting us to use their mining premises to perform the current investigation and LandTech's technical personnel for their help during the acquisition phase.

REFERENCES

Ashida, Y., 2001, Seismic imaging ahead of a tunnel face with three-component geophones: International Journal of Rock Mechanics and Mining Sciences, **38**, no. 6, 823-831.

Ashida, Y., T. Matsuoka, and H. Kusumi, 2001, Seismic imaging technique of looking ahead of tunnel face by use of 3 components receivers: Proceedings of Japan Society of Civil Engineers, no. 680, 123-129.

Bi, B.-K., 2009, The application of the electric method to Bauxite exploration: Geophysical and Geochemical Exploration, **33**, no. 4, 400-402.

Brückl, E., W. Chwatal, J. Dölzlmüller, and W. Jöbstl, 2001, A study of the application of VSP to exploration ahead of a tunnel: International Journal of Rock Mechanics and Mining Sciences, **38**, no. 6, 833-841.

Dragičević, I., M. Andrić, and I. Blašković, 1991, Geological-Geophysical exploration of the Bauxite deposits application on the shallow seismic reflection method: The Mining-Geological-Petroleum Engineering Bulletin, **3**, no. 1, 23-28.

Grodner, M., 2001, Delineation of rockburst fractures with ground penetrating radar in the Witwatersrand Basin, South Africa: International Journal of Rock Mechanics and Mining Sciences, **38**, no. 6, 885-891.

Inazaki, T., H. Isahai, S. Kawamura, T. Kurahashi, and H. Hayashi, 1999, Stepwise application of horizontal seismic profiling for tunnel prediction ahead of the face: The Leading Edge, **18**, no. 12, 1429-1431.

Lin, C. N., Y. Y. Jiao, and Q. S. Liu, 2006, Site Experiment for Predicting Hazardous Geological Formations ahead of Tunnel Face: Key Engineering Materials, **326-328**, no., 461-464.

Lüth, S., S. Buske, R. Giese, and A. Goertz , 2005, Fresnel volume migration of multicomponent data, Geophysics, **70**, no. 6, S121–S129.

Moser, T. J., 1991, Shortest path calculation of seismic rays: Geophysics, **56**, no. 1, 59-67.

Neishtadt, N. M., L. V. Eppelbaum, and A. G. Levitski, 2006, Application of piezoelectric and seismoelectrokinetic phenomena in exploration geophysics: Review of Russian and Israeli experiences: Geophysics, **71**, no. 2, B41-B53-B41-B53.

Nolet, G., 1987, Seismic wave propagation and seismic tomography, *in* G. Nolet, ed., Seismic tomography: with applications in global seismology and exploration geophysics: Reidel, 1-23.

Otto, R., E. Button, H. Bretterebner, and P. Schwab, 2002, The application of TRT - True reflection tomography - At the unterwald tunnel: Felsbau, **20**, no. 2, 51-56.

Sattel, G., P. Frey, and R. Amberg, 1992, Prediction ahead of the tunnel face by seismic methods - pilot project in Centovalli Tunnel, Locarno, Switzerland: First Break, **10**, no. 1, 19-25.

Tsai, D. T., F. L. Hwang, S. C. Kao, and L. P. Shi, 2005a, Application of resistivity image for the Hsuehshan Tunnel: International Symposium on Design, Construction and Operation of Long Tunnels, Taipei, Taiwan.

Tsai, D. T., F. L. Hwang, H. M. Shih, S. C. Kao, J. S. Tseng, and L. P. Shi, 2005b, Application of tunnel seismic prediction for the Hsuehshan Tunnel: International Symposium on Design, Construction and Operation of Long Tunnels, Taipei, Taiwan.

Tsourlos, P., G. Tsokas, and A. Yiamas, 2005, Derecting bauxitic lenses in galleries using geophysical techniques: Proceedings of the 2nd conference of the comitee of Economic Geology, Mineralogy, Geochemistry of the Greek geological Society, Thessaloniki, Greece, 7-9 October, 367-376. (In Greek)

Yamamoto, T., S. Shirasagi, Y. Yokota, and Y. Koizumi, 2010, Imaging geological conditions ahead of a tunnel face using Three-dimensional Seismic Reflector Tracing

System: International Journal of the Japanese Committee of Rock Mechanics, **6**, no. 1, 23-31.

Zhang, J., and M. N. Toksoz, 1998, Nonlinear refraction traveltime tomography: Geophysics, **63**, no. 5, 1726-1737.

CAPTIONS OF TABLES

Table 1: Recording parameters

Table 2: Data processing flow

CAPTIONS OF FIGURES

Figure 1: Map of Greece with the area of study and geologic formations encountered in the mine. The numbers correspond to (1) Flysh (2) Thin-bedded Limestones (3)compact (or crystallic) bitouminous limestones (4) Intermediate Limestones and (5) the Bauxite. (Diagram not to scale).

Figure 2: Source and receiver geometry for seismic imaging ahead of the gallery face.

Figure 3: Geometry of the survey and coordinate conversion.

Figure 4: Survey setup. Rhombus in D1 and D2 show the source points used and the geophones are depicted with the triangles with G1 up to G8. The arrows show the geophone components orientation.

Figure 5: (a) Raw seismic data as recorded for the 3C ahead of tunnel imaging. (b) the spectrum for the part of the seismic record traces before the arrival of the higher amplitude seismic waves.

Figure 6: Seismic data as recorded for the 3C ahead of tunnel imaging after processing.

Figure 7: The imaging results of equi travel time planes. (a) and (b) show a 3d view of the result with intersecting planes. In more detail the shown planes are depicted in (c) horizontal plane at the level of the source X=0 m, and 2 vertical planes with the interpreted reflections (e) at Y=0m and (f) at Y= -22m.

Figure 8: The full 3D imaging of equi-travel time planes

Figure 9: Seismic tomography survey setup. The circles show the shot points while the triangles show the geophones used.

Figure 10: Select seismic records obtained corresponding to the locations 6 and 36 as seen on figure 10.

Figure 11: Seismic tomography, P wave velocity section as well as the position of shots and geophones. The inserted picture shows the ray coverage.

Figure 12: (a) The results of equi travel time plane imaging at the level of the tunnels overlayed on the seismic tomography result. (a) as in a adding the location of the reflecting planes.

TABLE 1

Receivers	8 three-component geophones f_o= 28Hz
Channel number	24
Recording instrument	Geometrics Geode 24 bit
Receiver spacing	5m
Sampling interval	1000 ns
Record length	200 ms

TABLE 2

Field data format conversion
Spectral analysis
Band Pass filtering
AGC Trace equalization
Predictive deconvolution
Average velocity assessment
Reflector imaging

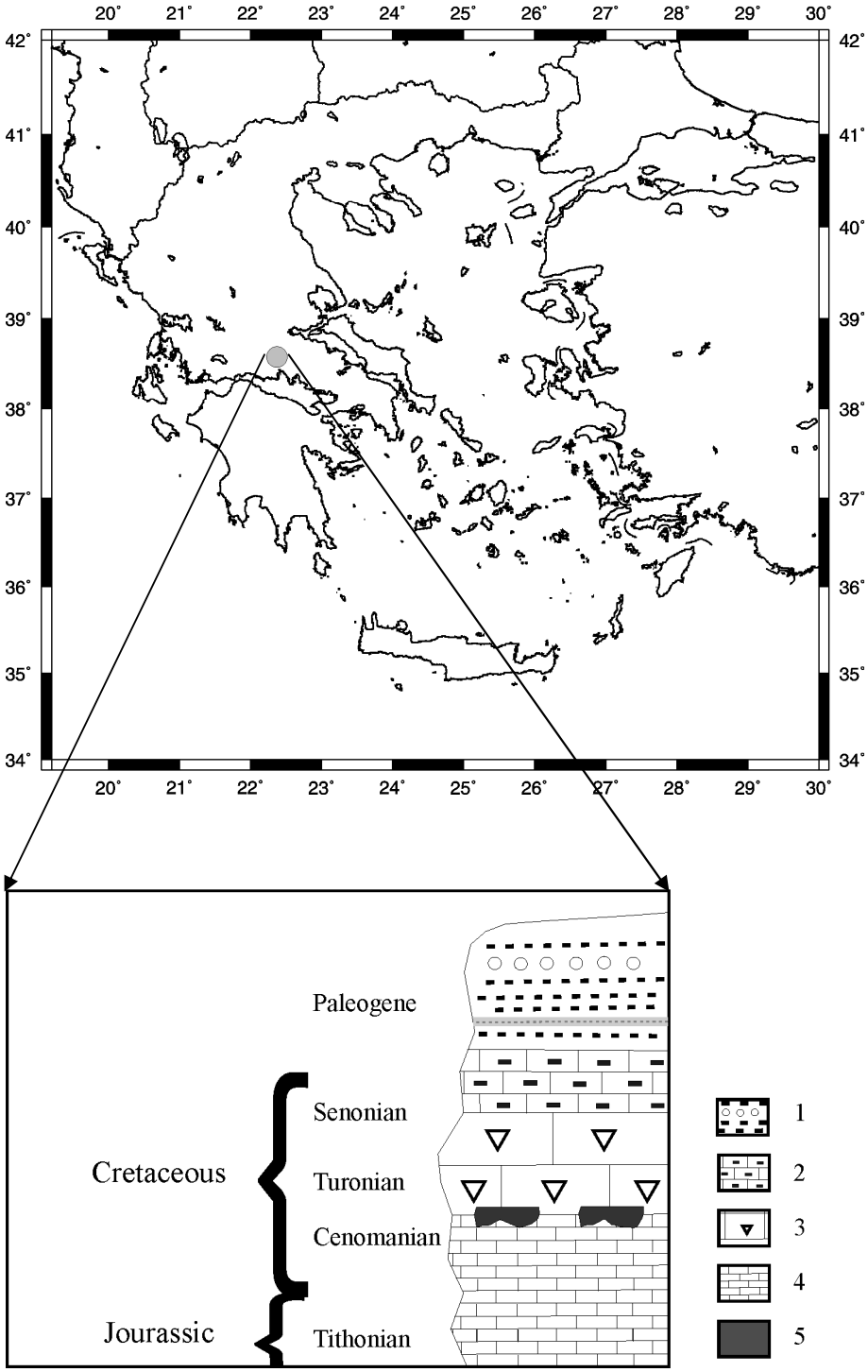
20°
21°
22°
23°
24°
25°
26°
27°
28°
29°
30°
42°
41°
40°
39°
38°
37°
36°
35°
34°
Paleogene
Senonian
Cretaceous
Turonian
Cenomanian
Jourassic
Tithonian
1
2
3
4
5

FIG.1

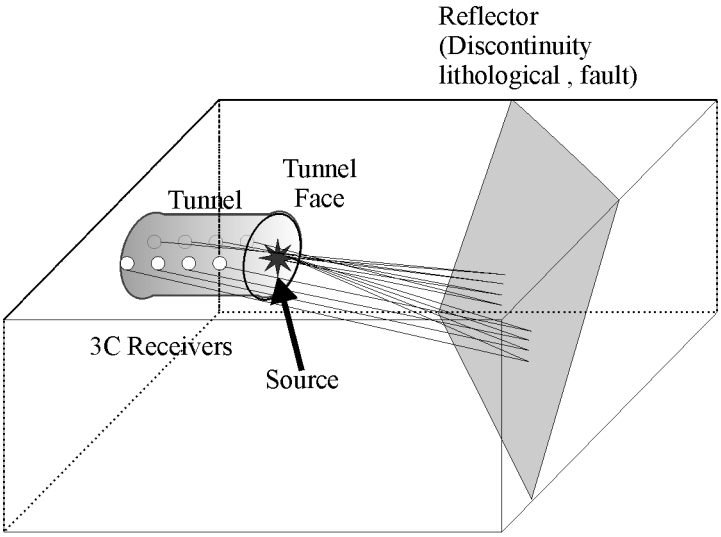
Reflector
(Discontinuity
lithological , fault)
Tunnel
Face
Tunnel
3C Receivers
Source

Figure 2

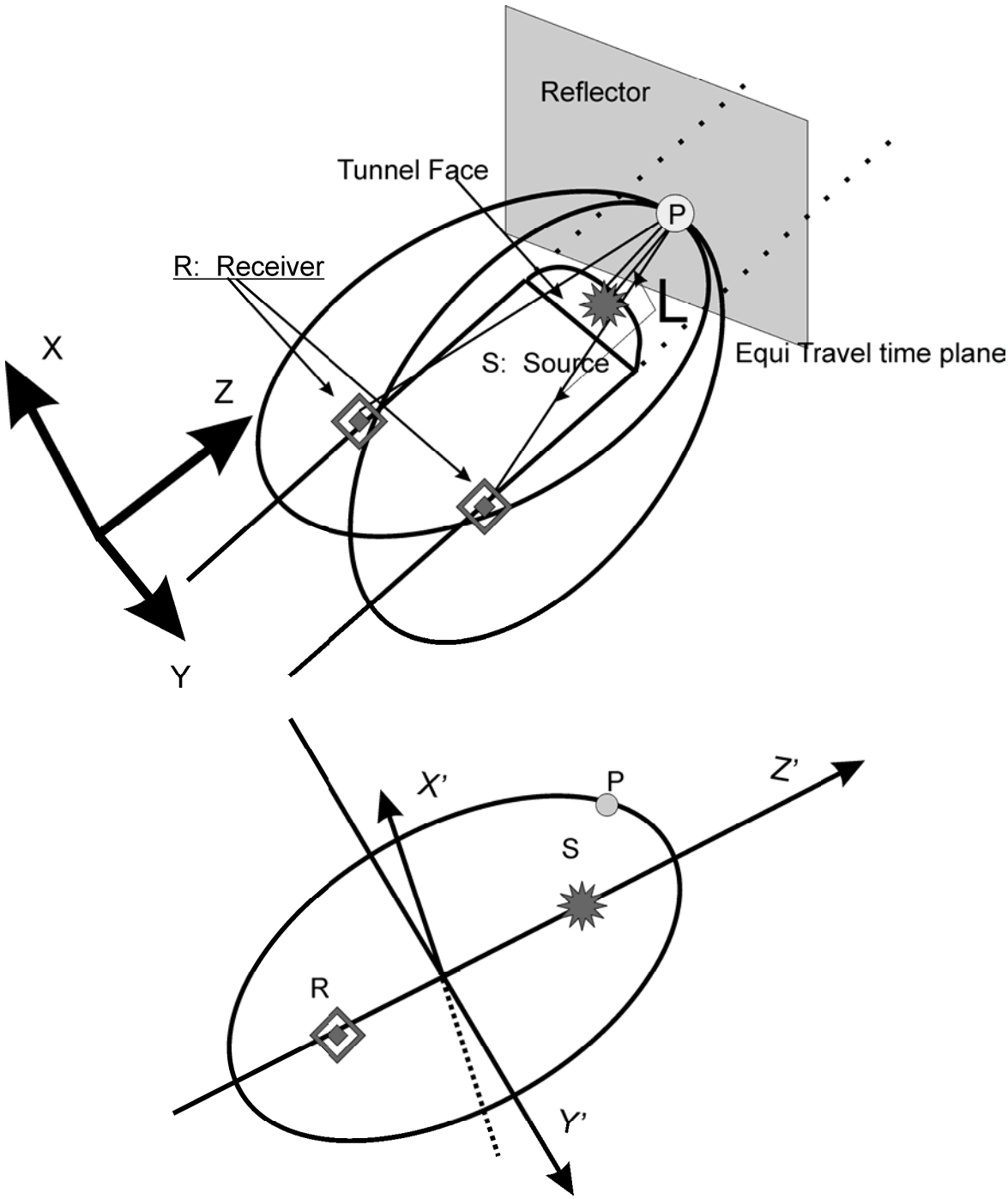
Reflector
Tunnel Face
P
R: Receiver
L
X
Z
S: Source
Equi Travel time plane
Y
X'
P
Z'
S
R
Y'

Figure 3

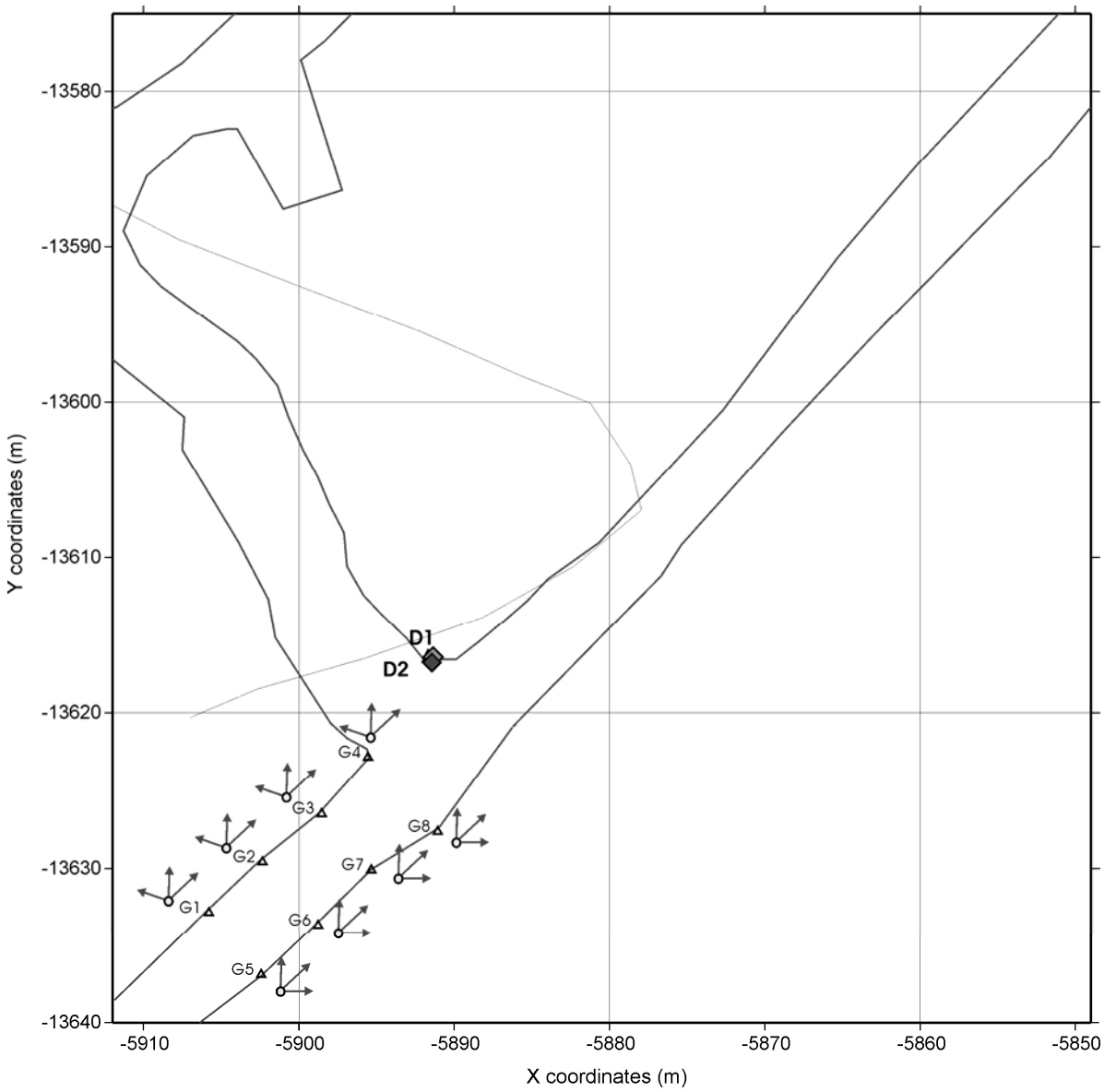
-13580
-13590
-13600
-13610
-13620
-13630
-13640
Y coordinates (m)
-5910
-5900
-5890
-5880
-5870
-5860
-5850
X coordinates (m)
D1
D2
G1
G2
G3
G4
G5
G6
G7
G8

FIG.4

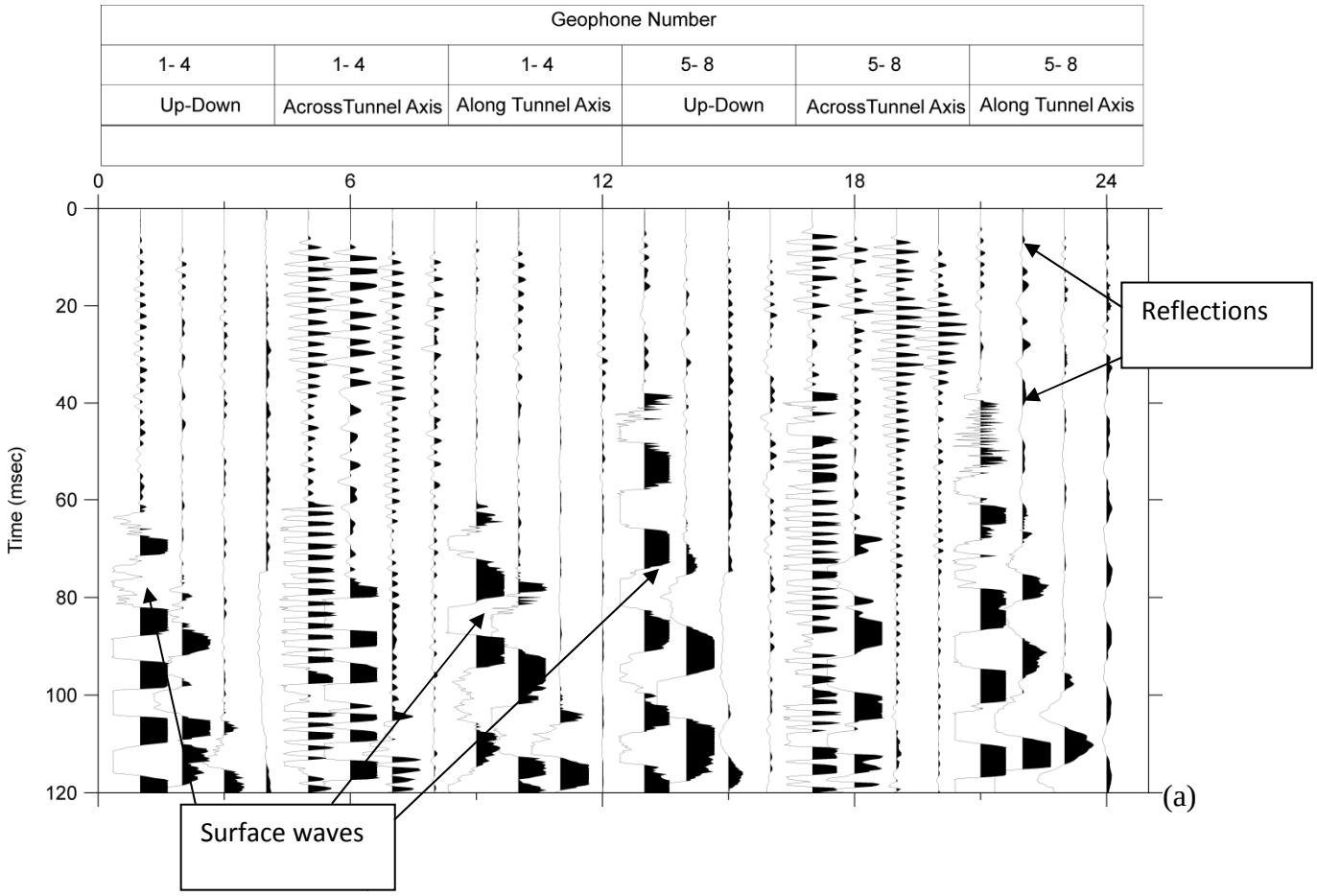
Geophone Number
1- 4
1- 4
1- 4
5- 8
5- 8
5- 8
Up-Down
AcrossTunnel Axis
Along Tunnel Axis
Up-Down
AcrossTunnel Axis
Along Tunnel Axis
0
6
12
18
24
0
20
40
60
80
100
120
Time (msec)
Reflections
Surface waves
(a)

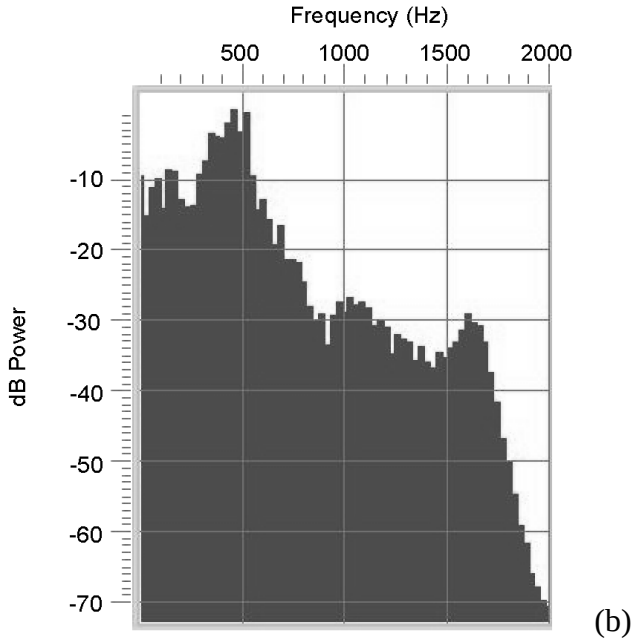
Frequency (Hz)
500
1000
1500
2000
-10
-20
-30
-40
-50
-60
-70
dB Power
(b)

FIG.5

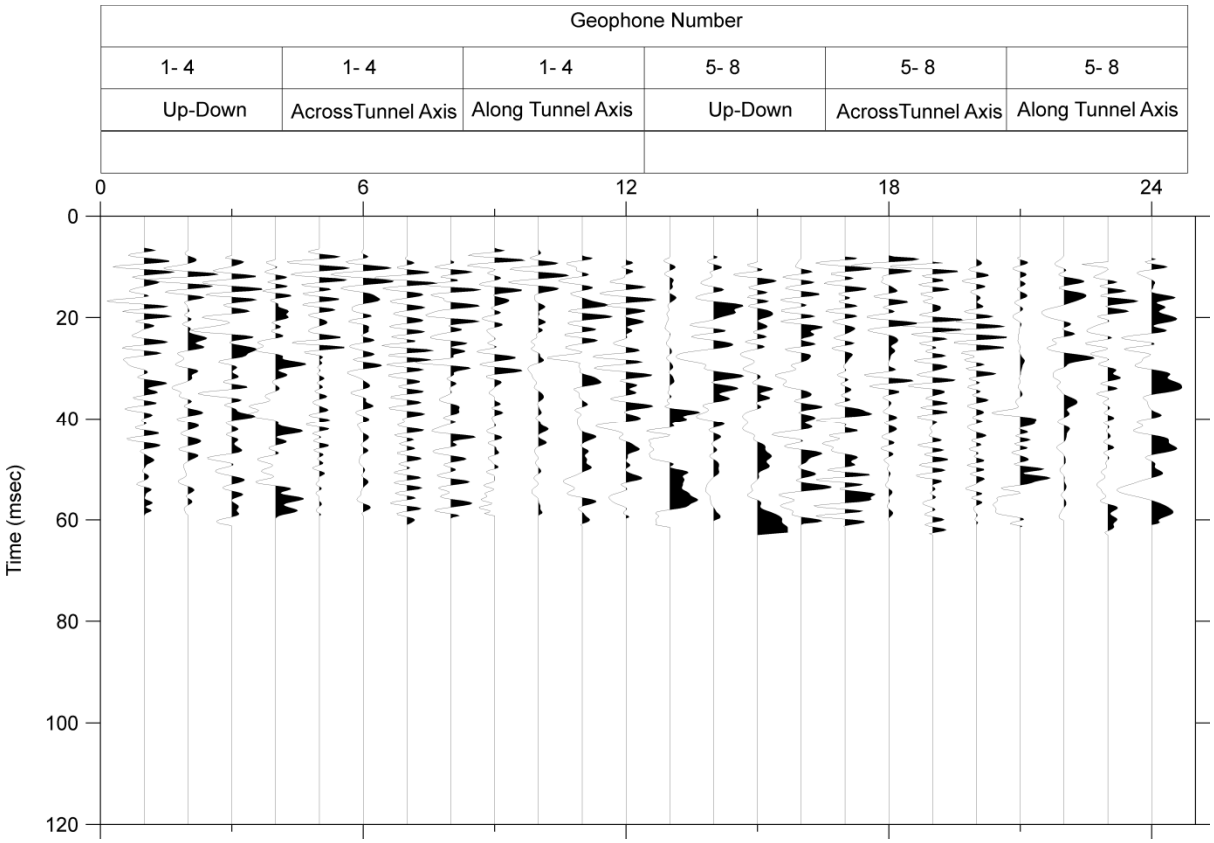
Geophone Number
1- 4
1- 4
1- 4
5- 8
5- 8
5- 8
Up-Down
AcrossTunnel Axis
Along Tunnel Axis
Up-Down
AcrossTunnel Axis
Along Tunnel Axis
0
6
12
18
24
0
20
40
60
80
100
120
Time (msec)

FIG.6

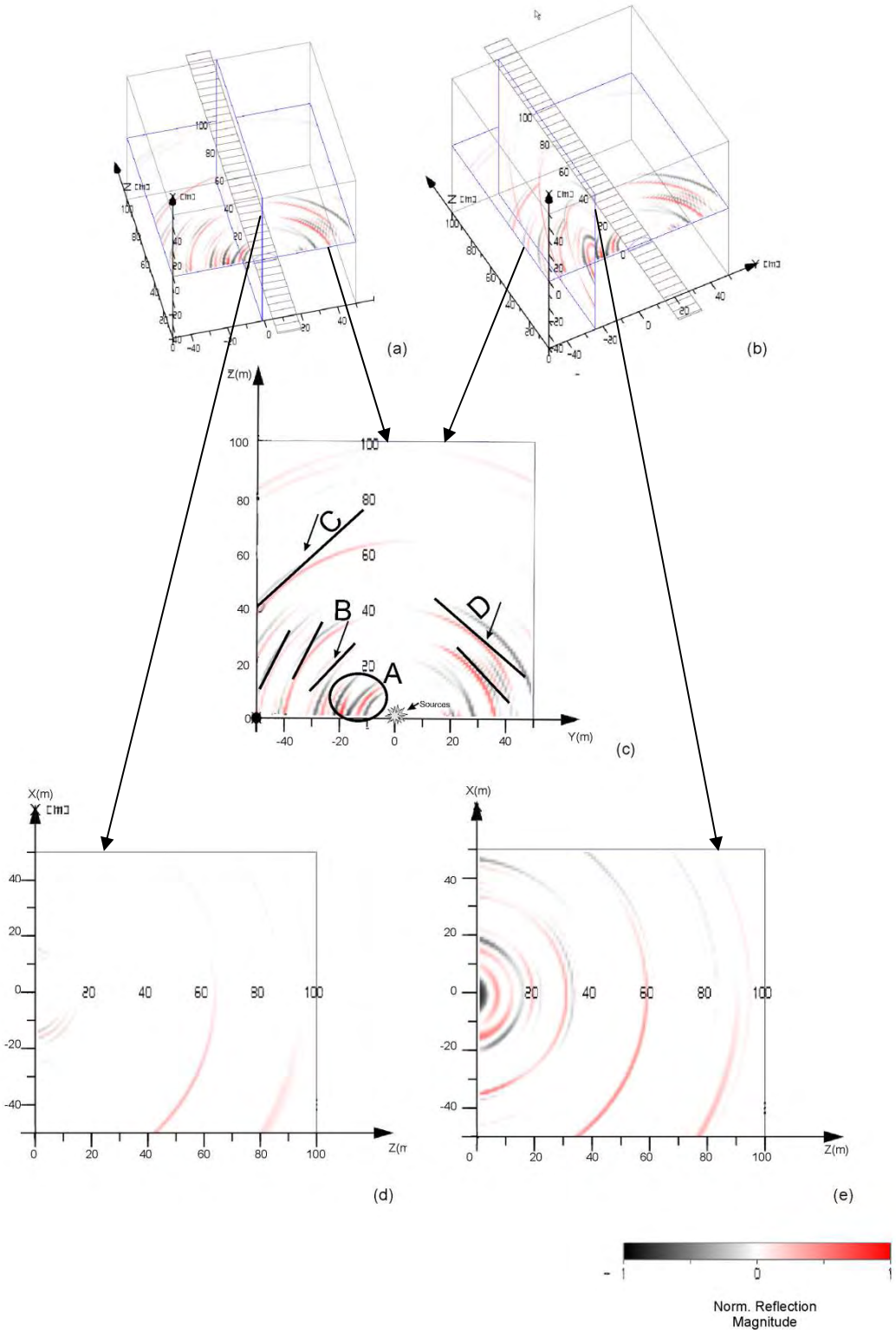
(a)
(b)
Z(m)
100
80
60
40
20
0
C
B
A
D
Sources
-40
-20
0
20
40
Y(m)
(c)
X(m)
(d)
(e)
Norm. Reflection
Magnitude

FIG.7

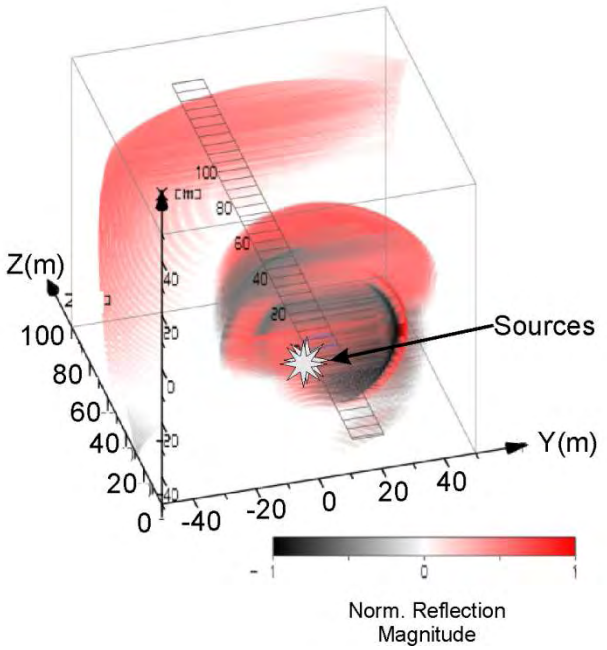
Z(m)
100
80
60
40
20
0
-40
-20
0
20
40
Y(m)
Sources
Norm. Reflection
Magnitude

FIG.8

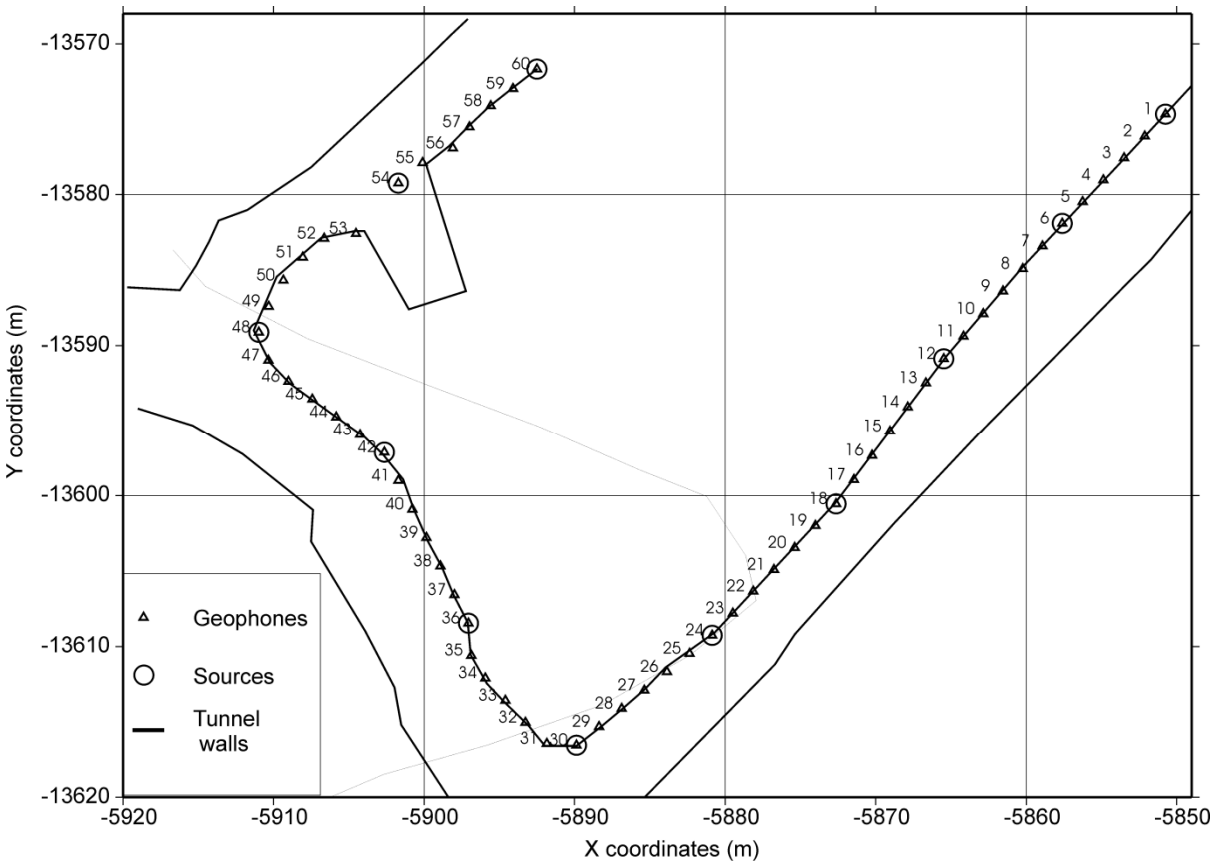
Y coordinates (m)
X coordinates (m)
-13570
-13580
-13590
-13600
-13610
-13620
-5920
-5910
-5900
-5890
-5880
-5870
-5860
-5850
Geophones
Sources
Tunnel walls

FIG.9

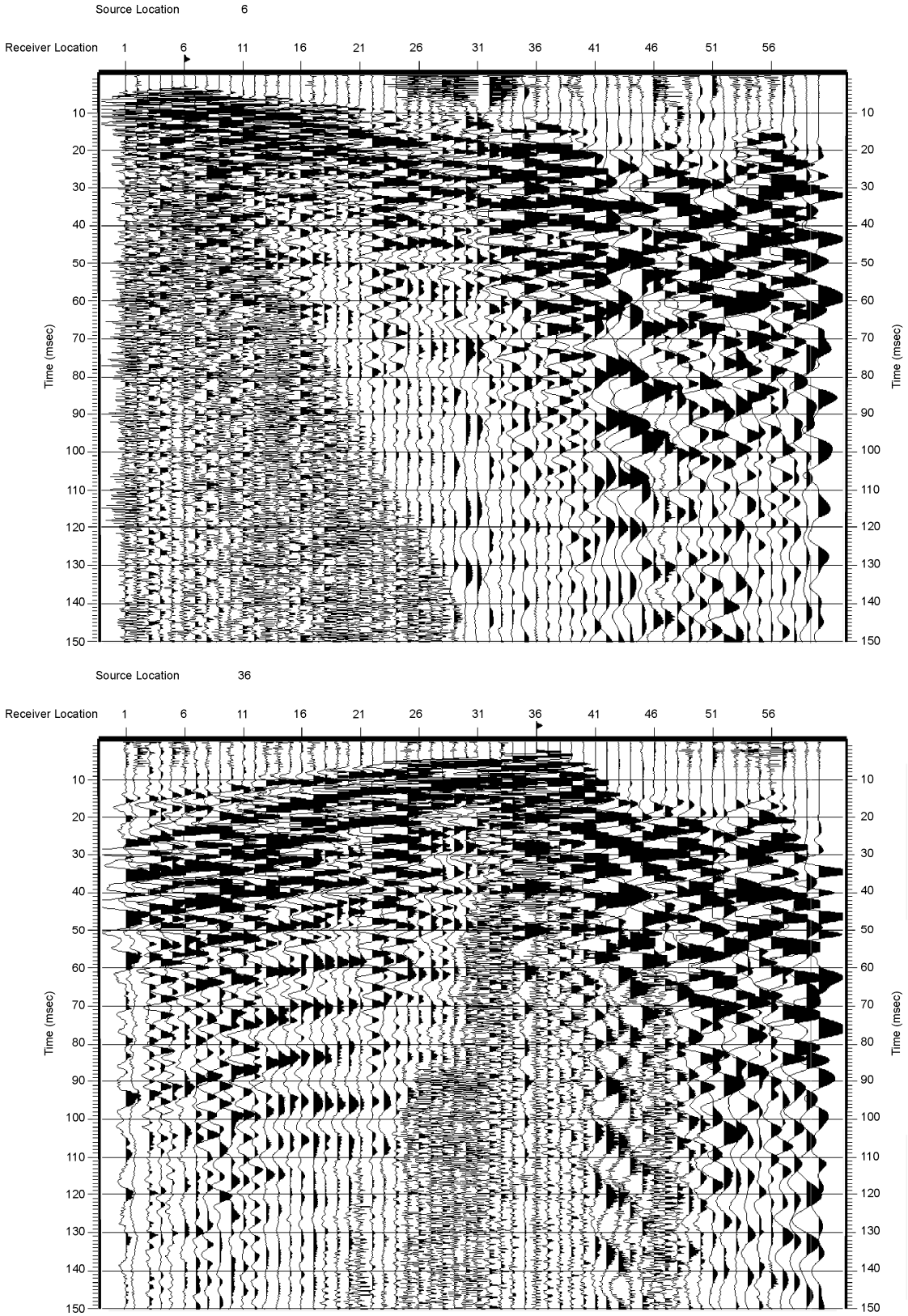
Source Location 6
Receiver Location 1 6 11 16 21 26 31 36 41 46 51 56
Time (msec) 10 20 30 40 50 60 70 80 90 100 110 120 130 140 150
Source Location 36
Receiver Location 1 6 11 16 21 26 31 36 41 46 51 56
Time (msec) 10 20 30 40 50 60 70 80 90 100 110 120 130 140 150

FIG.10

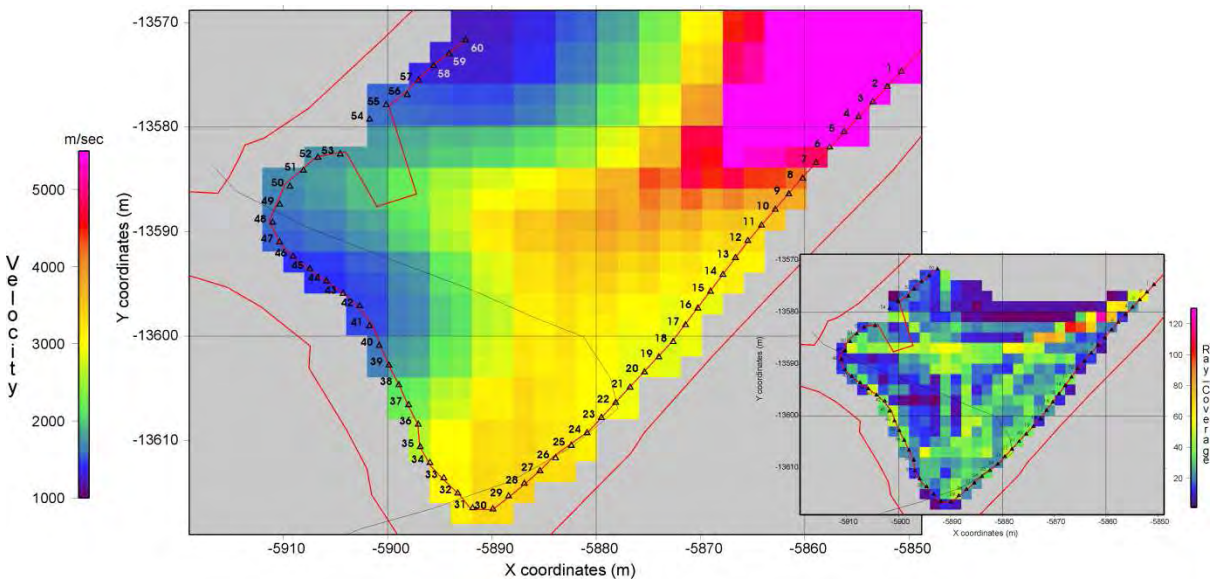

m/sec
Velocity
5000
4000
3000
2000
1000
Y coordinates (m)
-13570
-13580
-13590
-13600
-13610
X coordinates (m)
-5910
-5900
-5890
-5880
-5870
-5860
-5850
Ray_Coverage

FIG.11

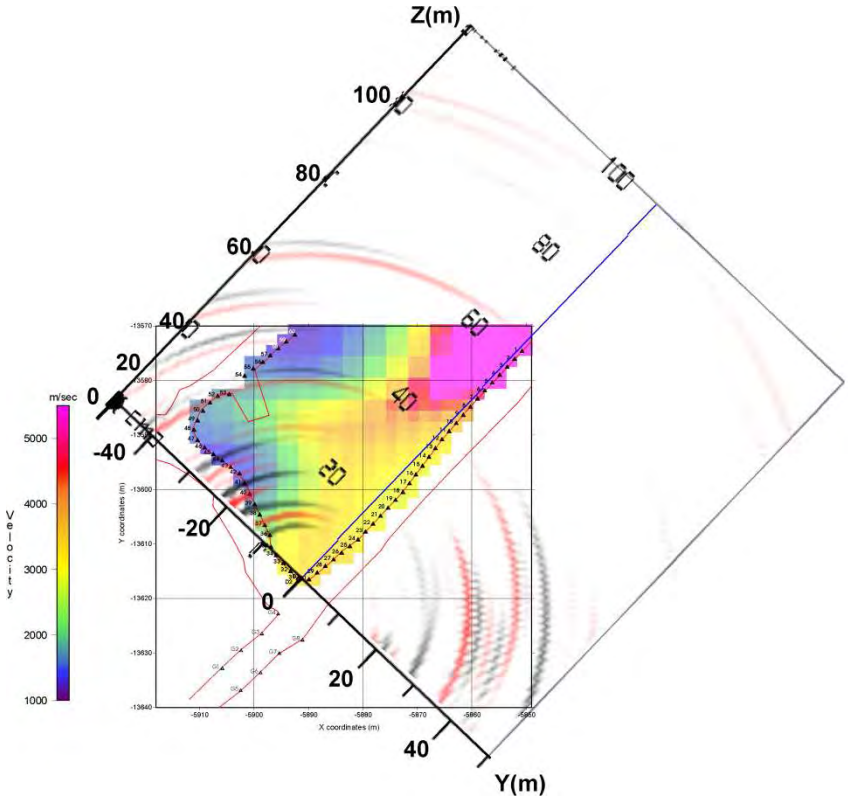
Z(m)
Y(m)
m/sec
Velocity
X coordinates (m)
Y coordinates (m)

(a)

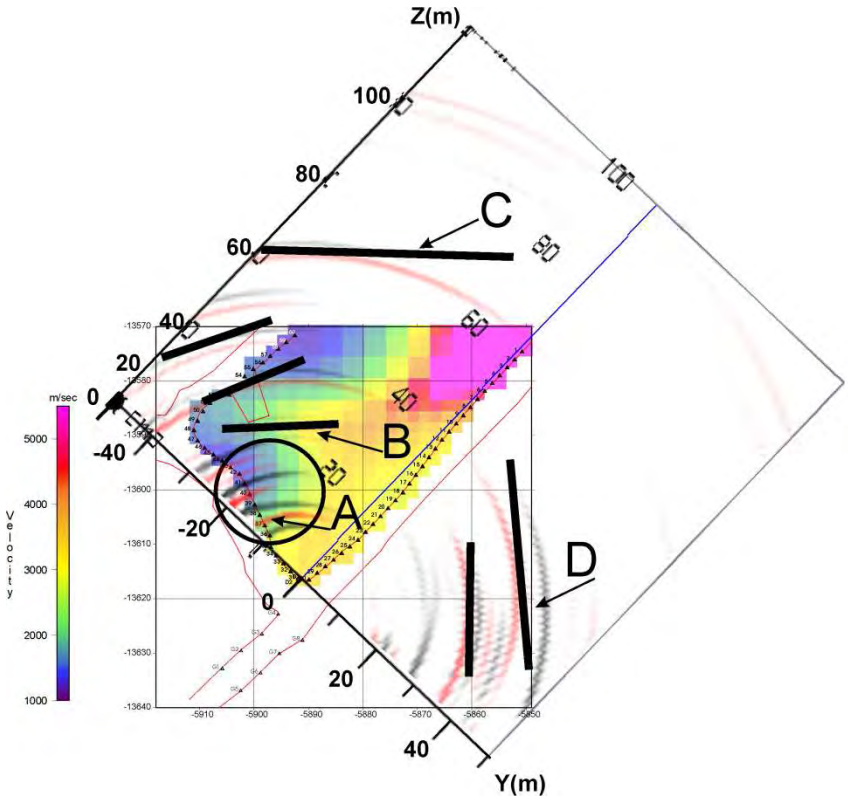
Z(m)
Y(m)
m/sec
Velocity
A
B
C
D

(b)

FIG.12